Journal of Materials Science: Materials in Engineering

ORIGINAL PAPER Open Access

Self-assembled rectorite films with remarkable mechanical performance: preparation, structural characterization, and properties

Maria T. Atanasova[1], Walter W. Focke[1*] and Theodor Loots[2]

Abstract

Cohesive flexible rectorite clay films with good mechanical performance were prepared by a simple casting method through the self-assembly of exfoliated natural clay from aqueous dispersions. The multi-layered microstructure of the films consisted of continuous layers of aligned clay platelets parallel to the casting surface. Layers overlap randomly in the lateral direction (plane) and join vertically in an irregular manner by edge-to-face cross-linkages (bridging) to form coherent multi-layered nanostructured films with platelet-void microstructure. The films with the highest mechanical properties had thicknesses below 30 µm. Overall films from rectorite clay with monovalent interlayer content exhibited a higher experimental tensile strength ranging up to 44 MPa and Young's modulus up to 56 GPa. The corresponding experimental values for films with divalent interlayer cations were 23 MPa for strength and 25 GPa for modulus. The highest experimental values for strength and modulus for neat Na–Ca–rectorite films were 25 MPa and 50 GPa respectively. These two mechanical property values of the best rectorite-based clay films compare favorably with values featured by polymer films typically used for packaging applications.

Keywords Rectorite, Clay films, Casting, Mechanical properties

Introduction

The need for "greener" alternatives to current engineering materials has focused research on sustainable resources and processes with a reduced impact on the environment (Zimmerman et al. 2020). Natural phyllosilicate minerals are among the available options used for polymer property enhancement in a growing array of applications (Abulyazied and Ene 2021; Long et al. 2022; Lopes et al. 2014). Suitably modified clays can radically improve the strength and stiffness of polymers even at low addition levels (ca. 5 vol.%). However, for best performance, it is a prerequisite that the clay be well dispersed in an extensively exfoliated form. The smectite group clay minerals, montmorillonite, and hectorite in particular, are the preferred reinforcement agents in polymer nanocomposites. They are easily modified to suit specific target functionalities because of their unique ion exchange capacity, reactive surface properties, lamellar crystal morphology, and favorable particle size and aspect ratio (Johnston, Santagata, and Sasar, 2022; Tjong 2006; Zhang and Evans 2012). Clay minerals are structurally analogous to some crystalline organic systems with similar lamellar arrangement, i.e., polyethylene (Ballard and Rideal 1983). Both organic and inorganic crystalline lamellae

*Correspondence:
Walter W. Focke
walter.focke@up.ac.za
[1] Department of Chemical Engineering, University of Pretoria, Private Bag X20, Hatfield 0028, South Africa
[2] Department of Statistics, University of Pretoria, Private Bag X20, Hatfield 0028, South Africa

have comparable dimensions and, due to the large aspect ratios, they tend to naturally form oriented structures in thin films, coatings, and membranes (Ballard and Rideal 1983). Hybrid inorganic materials and clay-containing films are trending topics in materials research (Ebina 2018; Fernandes et al. 2014; George and Ishida 2018; Johnston et al. 2022; Saha et al. 2022; R. Schoonheydt 2014; C.-H. Zhou, Shen, Liu, and Liu, 2011).

The platey morphology of clay minerals and their behavior in aqueous suspensions facilitates film formation on evaporation. When clay platelets settle they orient themselves to form brick-like microstructures analogous to that of nacre (Bennadji-Gridi et al. 2006; Cerbelaud et al. 2020; Sellinger et al. 1998). This natural tendency of clay platelets, to assume face-to-face parallel orientation when dried from suspensions, is the core principle of film formation by self-assembly (T. Liu et al. 2008; Walley et al. 2012). Hauser and Le Beau (E.A. Hauser and Le Beau 1938; E.A. Hauser and Le Beau 1939) first demonstrated the preparation of such clay-only films from bentonite gels. The so-called Alsifilm (aluminum silicate film) was developed as a replacement for mica in electrical applications including insulation (Anon 1939). Numerous investigators (Ballard and Rideal 1983; Bennadji-Gridi et al. 2006; Minker-Villemin et al. 1998; Nam et al. 2007; Nam et al. 2009a, b; Nam et al. 2009a, b; Walker and Garrett 1967; Walley et al. 2012) extended the work of Hauser and Le Beau. Since then, many others (Cheng et al. 2017; Eguchi et al. 2022; Gogoi and Raidongia 2018; M.-L. Liu et al. 2018; Pan et al. 2018; Pujala et al. 2018; Shao et al. 2015; Wang et al. 2013; Wang and Lin 2014; Xiao et al. 2017; Y. Zhou et al. 2019) have investigated the preparation freestanding clay-only films by various means. Walley et al. (2012) confirmed that the simplest way, to obtain nanocomposites similar to the microstructural arrangements seen in nacre, was to allow dilute clay suspensions to evaporate by slow drying. Progress in this regard was recently reviewed (Saha et al. 2022).

This investigation explored the ability of natural rectorite, and its ion-exchanged modifications, to form self-standing, mechanically strong clay-only films. The primary goal was to develop a simple energy-efficient, environmentally-friendly process and evaluate the extent of process and product property limitations. The films were prepared by a casting process in the absence of binders, organic modifications, or thermal pre-treatments.

Rectorite is a 2:1 regular interstratification of mica-smectite type with d-spacing in the range 2.2 to 2.4 nm for single- and double water layers respectively (Atanasova et al. 2016; Xie et al. 2020). The flakes are made up of alternating non-expandable (mica-like) and expandable (smectite-like) layers in a 1:1 ratio. The swelling of the structure is facilitated by the hydration of the exchangeable cations in the montmorillonite-like interlayers. The mixed-layer structure of rectorite defines a set of unique properties that differ from those of mica and smectite alone. Water dispersions of rectorite clay easily form gels that spontaneously assemble into self-supporting cohesive films upon drying. The present study was a first step towards exploring the possibility of using rectorite clay to prepare non-isotropic (i.e., two-dimensionally oriented) nanocomposites with very high clay loadings, i.e., nacre-inspired nanocomposites. This communication addresses the ion exchange modification of rectorite and the optimization of processing conditions for film preparation by the evaporation method. Characterization and physical properties of these mechanically robust clay-only films are presented with a statistical evaluation of the limits for their ultimate mechanical performance.

Materials and methods

Materials

Raw rectorite samples were sourced from the Beatrix mine, South Africa, on three different occasions. Details regarding the purification, the cation exchange methodologies, and the various sample preparation procedures were reported elsewhere (Atanasova et al. 2016). The empirical formula of the Beatrix rectorite (Atanasova et al. 2016) is the following: $(Na_{0.76}Ca_{0.44}K_{0.13})[Al_{4.03}Ti_{0.03}(Fe,Mg)_{0.006}](Si_6Al_2)O_{20}(OH)_4.nH_2O$ corresponding to an average CEC of 45 mEq/100 g. The exchangeable interlayer (composition $Na_{0.10}$ $Ca_{0.13}$) has a layer charge of −0.36 per $O_{20}(OH)_4$ and the fixed interlayer (composition $Na_{0.66}$ $Ca_{0.31}K_{0.13}$) has a total charge of −1.41 per $O_{20}(OH)_4$. All the ion-exchanged modifications, used for the preparation of the films, were derived from purified rectorite sample labeled RT3 (Table 1). The exchange with Na^+ and Ca^{2+} cations produced nearly homoionic Na-rectorite and Ca-rectorite material respectively.

Table 1 XRD estimated mineralogical composition of purified rectorite (wt.%)

Mineral/sample	RT1	RT2	RT3
Rectorite	91.27	86.32	91.45
Quartz	3.21	5.64	5.95
Calcite	0.66	n.d	n.d
Muscovite	n.d	2.93	1.66
Chlorite	4.86	2.44	1.52
Pyrophyllite	n.d	2.66	n.d

Film preparation

Rectorite clay films were prepared by a suspension-casting process. The aqueous clay dispersions were poured into shallow pans and allowed to evaporate and dry slowly at ambient conditions. Aqueous suspensions of the purified rectorite clays and the ion-exchanged Li^+, Na^+, NH_4^+, K^+, Cs^+, Mg^{2+}, Ca^{2+}, Sr^{2+}, and Ba^{2+} modifications of sample RT3, were prepared in the concentration range 1.0 to 5.8 wt.%. Parameters such as clay concentration, sonication time, stirring time, and the nature of the casting pans were varied to tune the method for optimum mechanical performance of the films.

Prior to film casting all suspensions were ultrasonically dispersed in ultra-pure water for either 5 or 30 min using a Braun Labsonic sonicator fitted with a 2000 U probe. The instrument settings were optimized experimentally by the interactive measurements of the degree of dispersion, i.e., obscuration in a particle sizer. In order to prevent overheating, low power output settings were selected, i.e., the instrument amplitude dial was set close to the minimum, and a duty cycle of 1 was chosen. After sonication, the suspensions were cast immediately or subjected to further agitation by stirring for either 4 or 24 h before casting. Both the particle size (as a proxy for the degree of exfoliation) and the intrinsic stability (indicated by the zeta potentials) of the suspensions were monitored.

Characterization methodology

Particle size and *zeta potential* were determined using a Malvern Zetasizer Nano ZS system (Malvern Instruments Ltd, Malvern, UK). The zeta potential (ζ-potential) was calculated from the electrophoretic mobility (u_e) of rectorite particles using the Smoluchowski equation. All measurements were performed at 25.0 ± 0.1 °C, with an attenuation in the range 5–6. The pH of the suspensions was also recorded. Reported ζ-potential values represent an average of three measurements. The size of the dispersed particles in the sub-micron region was determined by the dynamic light scattering (DLS) technique using the same instrument and the reported values represent the number mean size. The dynamic light scattering polydispersity index (PDI) exceeded 0.1, i.e., the system had a moderate to broad polydispersity in which case size distribution by volume is considered meaningless.

Scanning electron microscopy (SEM). Film specimens were freeze-fractured while immersed in liquid nitrogen. Prior to examination they were mounted and coated with carbon. The imaging was performed on the fractured profiles as well as on the top and bottom surfaces of the films. A high-resolution field emission SEM (HR FEGSEM Zeiss Ultra Plus 55) with an InLens detector at acceleration voltages of 1 kV was used to ensure maximum resolution of surface detail.

X-ray diffraction (XRD) analysis was carried out on a Bruker D8 Advance diffractometer with 2.2 kW CuKα radiation (λ = 1.54060 nm), LynxEye detector with an active area of 3.7° and Ni filter. Dry film samples were scanned from 2 to 36° 2θ in step scan mode at a speed of 0.02° 2θ steps size/5 s and generator settings of 40 kV and 40 mA. Rietveld refinements were done with DIFFRAC. TOPAS V4.2 software using the fundamental parameters approach (FPA) (Cheary and Coelho 1992). The volume-weighted mean crystallite size (LVol-IB in TOPAS language) was calculated from refined data based on intermediate crystallite size broadening modeled by a Voigt function. The method incorporated by TOPAS uses integral breadths and a domain-size broadening model (Stokes and Wilson 1942).

BET analysis. The specific surface areas of the cast films were determined on a Micromeritics Flowsorb II 2300 and a Nova 1000e BET instrument in N_2 at 77 K.

Tensile testing was performed on an Ametek Lloyd Instrument LRX Plus single-column tensile tester fitted with a 50-N load cell. Film thickness was measured using a Mitutoyo Digimatic micrometer with a measurement precision of ± 0.2 μm. The average of multiple measurements taken along the test strip is reported. Film strips with dimensions 100 mm long and 10 mm wide were cut and conditioned in a desiccator at room temperature for at least 48 h prior to measurements (ASTM and International, 2012, 2013a, 2013b). The humidity in the desiccator was maintained at ca. 55% RH by the presence of a saturated $Ca(NO_3)_2 \cdot 4H_2O$ solution. The ends of the strips were sandwiched between two pieces of carton before clamping in the grips of the tensile tester. The gauge length (grip separation) is set at 75 mm. The tensile tests were conducted at a draw speed of 20 mm min^{-1}. At least three tensile test strips were obtained and tested per cast sample film. The maximum recorded value is reported together with the overall standard deviation. This approach was followed as the objective was to determine the ultimate strength of these types of films.

The presently measured mechanical property values did not represent the intrinsic values that can potentially be attained. This is because of the many flaws and defects in the films caused by the limitations of the preparation methods. The measurement process itself was flawed including the way the samples were clamped. Therefore, a statistical analysis was performed to estimate the likely limits for the ultimate material properties. Details of this analysis are presented in the Supplementary Information.

Results

The primary focus of this study was to find the best rectorite clay derivative (obtained via ion exchange) and to optimize the preparation method (slurry-solids content, ultrasonication conditions, etc.) for maximum strength or stiffness of the cast inorganic clay films. In this process, a large number of film samples (247) were prepared and tested. The full set of experimental conditions, and the properties of the resultant films, are provided in the Excel spreadsheet associated with this communication. This document lists the physical properties of the particle suspensions employed, the processing conditions, and the tensile properties of the cast films that were obtained.

Processing conditions and properties of the clay suspensions

For each ion-exchanged clay sample, the film that featured the best mechanical properties, and the procedures that were used to prepare it, were identified. Additional measurements were performed on the parent slurry as well as the resultant films. Table 2 describes the processing conditions and the physical properties of the corresponding clay suspensions together with the pH, ζ-potential, and the mean particle size. In what follows, an attempt is made to link the best film mechanical properties to the process conditions that made them possible.

Upon casting, the divalent suspensions settled relatively quickly and at similar rates. However, those from the purified neat material and monovalent-exchanged samples formed more or less viscous gels at higher solid loadings. The particle size distributions of all the suspensions featured moderate to broad polydispersity indices (PDI > 0.1) for which the D_{10}, D_{50}, and D_{90} particle diameters are reported in Table 2. The neat and monovalent rectorite suspensions produced stable colloidal systems with ζ-potential values below – 30 mV. Lithium and sodium-containing dispersions with ζ-potential values – 52 mV and – 49 mV respectively did not settle before full evaporation. These films also took a longer time to dry. The divalent suspensions showed electric potential shifts towards less negative values, i.e., above – 30 mV where agglomeration typically commences. This is supported by the experimental observation that they had a higher tendency to flocculate.

The size of the exchangeable interlayer cation also had an effect on the suspension flocculation rate. Cations larger than Na^+ exhibited progressively less stable suspensions that readily re-aggregated after dispersion. The neat rectorite suspensions with mixed Na–Ca–ion interlayer showed stability similar to that of monovalent rectorite modifications. The RT1 suspension featured a lower ζ-potential probably due to the higher pH of 8.5 caused by the presence of calcite as an impurity. The ζ-potential increased with the increase in the pH for the monovalent rectorite modifications. However, the Mg-rectorite, with pH 8.2, dropped towards lower negative values. These results indicate a strong dependence of the electrostatic behavior of rectorite colloidal systems on the ionic composition in agreement with previous reports for Na- and Ca-forms of smectite (Chorom and Rengasamy 1995; Kaya and Yukselen 2005). Interestingly, the largest ions of both groups, i.e.,

Table 2 Processing conditions and physical properties of slurries that yielded rectorite films with the highest mechanical performance. In all cases, the solids content was 1.0 g clay/100 mL and the sonication time was 30 min (except for RT1 where it was 5 min)

Cation	Stirring time	pH	Zeta potential,	Particle size, μm		
	h		mV	D_{10}	D_{50}	D_{90}
Li	0	9.62	− 52.3 ± 0.9	3.07	8.41	775
Na	4	8.58	− 48.5 ± 0.3	2.71	5.83	17.9
NH_4	4	7.10	− 38.7 ± 1.8	3.56	8.91	547
K	4	8.80	− 43.7 ± 0.3	3.04	6.41	13.4
Cs	0	5.50	− 31.4 ± 1.6	2.96	5.42	9.97
RT1	24	8.50	− 34.8 ± 0.4	0.12	10.8	1045
RT2	24	6.70	− 46.5 ± 1.7	3.11	6.99	17.3
RT3	4	7.00	− 47.6 ± 0.2	3.30	6.96	15.5
Mg	24	8.22	− 20.6 ± 2.5	0.11	3.21	20.4
Ca	4	6.10	− 25.9 ± 0.9	3.24	7.27	17.4
Sr	0	6.20	− 27.2 ± 0.3	2.76	5.66	11.97
Ba	0	6.80	− 30.8 ± 0.8	2.73	5.70	13.8

monovalent Cs^{+}, and divalent Ca^{2+}, Sr^{2+}, and Ba^{2+} had ζ-potentials approaching the critical system stability boundary value, bordering lowest values for the former and highest for the latter at the same clay concentrations and pH below 7. These results suggest that the net negative charge is affected by the pH of the suspensions and that it plays a role in the behavior and stability of rectorite dispersions.

Film characterization and properties

The tensile properties of clay films from neat- and ion-exchanged rectorite modifications are presented in Table 3. In all cases the strain at break was very small, seldom exceeding 2%. Visual observations revealed that most samples failed by either developing a tear that started at an edge defect or right at the end where the sample was gripped. This means that the intrinsic mechanical properties were not achieved. Rather, the measured values were significantly influenced by the numerous defects present in the cast films, e.g., caused by handling during testing, and perhaps even small alignment errors when they were clamped into the tensile tester.

Table 3 Average and best mechanical property values obtained for rectorite-derived clay films. The reported film thicknesses correspond to the films which achieved the highest tensile strength

Cation	Film thickness	Tensile strength, MPa		Young's modulus, GPa	
	μm	Mean	Max	Mean	Max
Li	23	5.9 ± 3.3	12.9	7.2 ± 11.4	50.7
Na	23	7.9 ± 7.0	31.8	5.1 ± 10.0	55.3
NH_4	22	8.9 ± 8.1	43.7	4.1 ± 7.9	47.3
K	13	11.9 ± 10.5	35.7	9.3 ± 15.8	56.3
Cs	31	6.0 ± 4.9	15.5	11.6 ± 14.2	43.4
RT1	25	13.4 ± 5.6	23.9	7.4 ± 9.7	44.3
RT2	20	8.1 ± 3.2	11.7	19.7 ± 16.3	49.8
RT3	20	8.5 ± 5.1	24.6	4.2 ± 4.0	18.6
Mg	20	5.7 ± 4.4	13.9	4.8 ± 5.8	20.6
Ca	23	8.5 ± 6.4	22.9	9.2 ± 7.5	20.2
Sr	30	4.1 ± 2.4	8.0	4.1 ± 4.4	18.0
Ba	30	10.0 ± 2.7	14.9	8.7 ± 7.8	25.4

The measured tensile strength and modulus values for neat rectorite films varied from 12 to 25 MPa and 9 to 50 GPa respectively. Those from the ion-exchanged modifications ranged from 8 to 44 MPa and 19 to 56 GPa respectively. The films obtained from monovalent cation forms performed notably better (ranging from 13 to 44 MPa and 43 to 55 GPa) than those made with rectorite modified with divalent ions (tensile strength 8 to 23 MPa and modulus 18 to 25 GPa) (Table 3). Those made from the NH_4–rectorite also showed excellent tensile properties with strength and modulus values reaching 44 MPa and 47 GPa respectively. Amongst the large set of films with thicknesses ranging up to 150 μm, those with a tensile strength exceeding 5 MPa were less than 65 μm thick. The films that featured the highest strengths invariably had a thickness of less than 30 μm. The plot in Fig. 1 actually suggests an inverse thickness dependence for both tensile strength and Young's modulus if the envelope, defined by the best experimental values, is considered. Bennadji-Gridi et al. (2006) observed a similar trend for montmorillonite-based clay films obtained by the casting-evaporation method. They found that the bending strength of thinner films fell in the range of 112 ± 12 MPa while the values obtained for thicker films were lower than 45 MPa. This loss in performance was

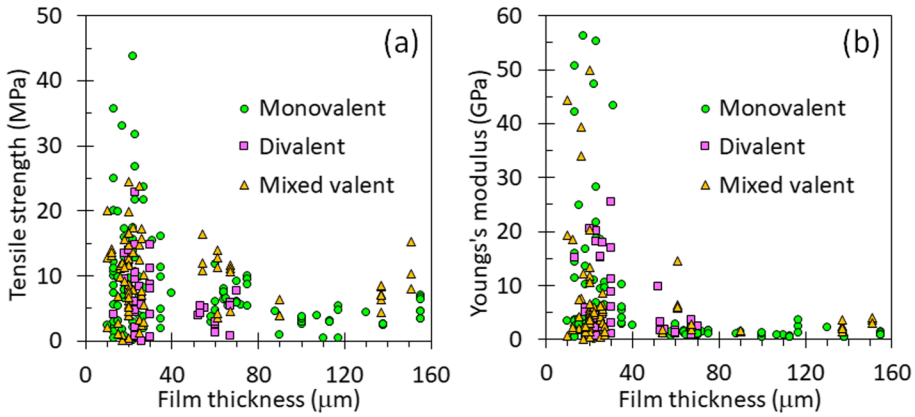

Fig. 1 The effect of film thickness on the mechanical performance of rectorite films (based on all 247 measurements)

attributed to the higher likelihood of defects, e.g., surface cracks, in the thicker samples.

The films with the best tensile properties did not necessarily originate from suspensions prepared under the same dispersion conditions. However, the dispersion regime of sonicating for 30 min with subsequent stirring for 4 h, proved most effective for producing strong films from each of the three groups—monovalent, divalent, and neat rectorite. The exceptions are RT1 where 5 min sonication followed by 24 h stirring, and RT2 and Mg^{2+}-films with 30 min sonication followed by 24 h stirring yielded the best results. Dispersions of Li^{+}- and Cs^{+}-based films and divalent Sr^{2+} and Ba^{2+} proved more suited to cast after 30 min sonication without stirring.

The data show considerable scatter in both the strength and the modulus characteristics of the rectorite films (Fig. 1 and Table 1). Significant variability was found, not only between films from different rectorite modifications but also within ion-exchanged samples, notwithstanding all attempts made to strictly control the processing parameters used in the film preparations.

All films had an off-white color with a subtle blue-grey tint and pearly luster on the smooth bottom side. Those obtained from neat rectorite were translucent (Fig. 2a). Films also displayed a noteworthy flexibility allowing folding and bending. Creasing was possible for the thin films obtained from neat and monovalent-exchanged rectorite (Fig. 2b).

SEM micrographs of multilayer textured rectorite films reveal a microstructure defined by more-or-less planar orientations of the flakes (Fig. 3). The clay platelets are arranged parallel to each other in continuous layers (Fig. 3). The platelets randomly bend and join neighboring layers through edge-to-face contacts resulting in structured, coherent sheets (Fig. 3c, d). This geometrical model produces a random but somewhat complex network of cavities of variable shape and size.

All films exhibit unevenly frayed fracture surfaces with a rather curved profile pattern. The upper sections of the films showed a lightly waved structure comprising finely layered parallel clay sheets that appeared more tightly stacked compared to the more ruggedly textured middle and base sections. This appears to be an artifact of particle size segregation that occurred during the gravity-driven settling of clay platelets on drying. The top section is layered with the thinnest particles which were the last to assemble during evaporation. These flakes have the most favorable aspect ratio to align into compact sheets with the highest surface-to-volume ratio. This anisotropic texture is less pronounced in the neat and monovalent clay films. In contrast, the films obtained from divalent rectorite featured larger undulations throughout the film cross-section profile with visibly more loosely assembled sheets (Fig. 3d, f). Similar effects of the interlayer content on the microstructure of clay films were previously observed (Nam et al. 2009a, b) and attributed to differences in the susceptibility of the ion modifications to delaminate an aggregate in aqueous suspensions.

The anisotropic structure of the film texture had a direct effect on the performance characteristics, especially the damage tolerance. For instance, rectorite films with thickness exceeding 20 µm were significantly less flexible and tended to fracture more easily on bending. Folding distorts the orientation of the sheets, and this is typically initiated at the weekly textured base of the films made up of larger loosely connected particles. Eventually

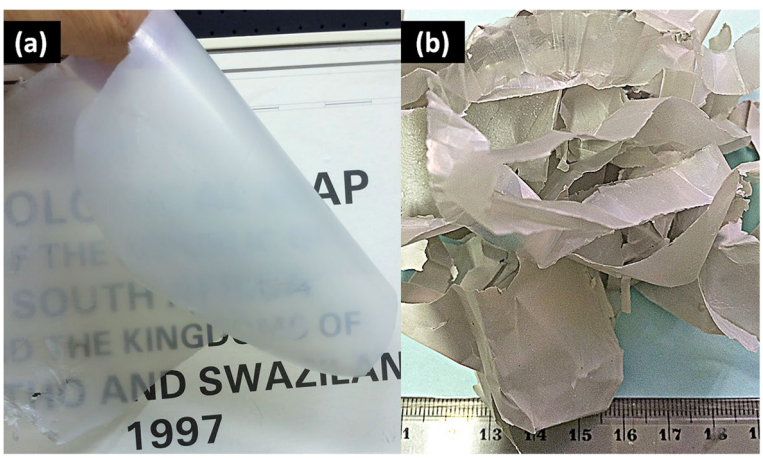

Fig. 2 **a** Illustrating the transparency, of translucent flexible films made from purified rectorite clay without the use of additives or binders, and **b** the flexing, bending, and creasing of ribbons offcuts. The film thickness was 8.0 µm in both cases

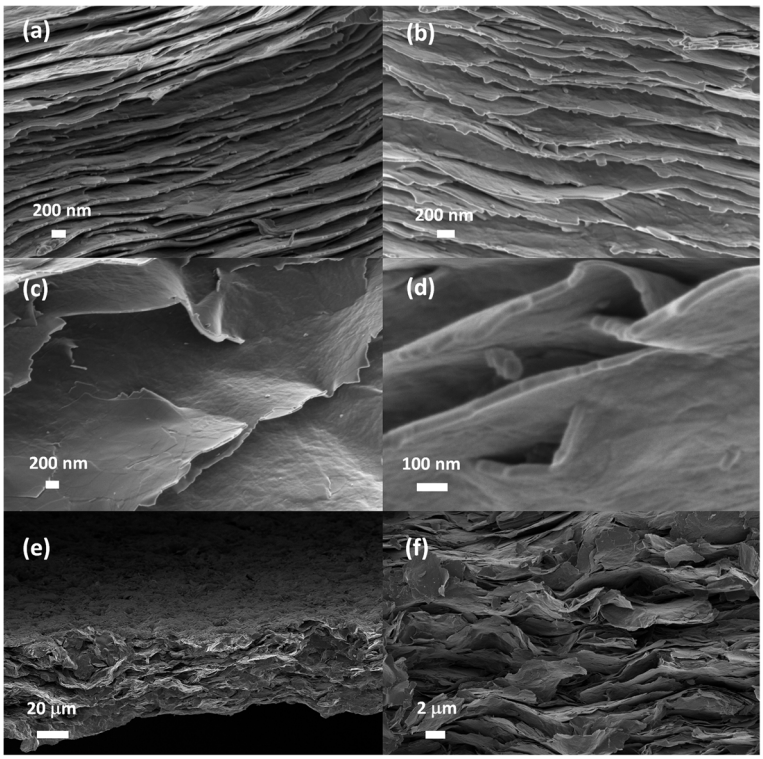

Fig. 3 SEM micrographs showing a cross-section view of rectorite films from raw purified clay **a** and **b**; Li^{+}- (**c**) and Na^{+}-exchanged rectorite (**d**); Mg^{2+}- (**e**) and Ba^{2+}- modified, **f** rectorite clay

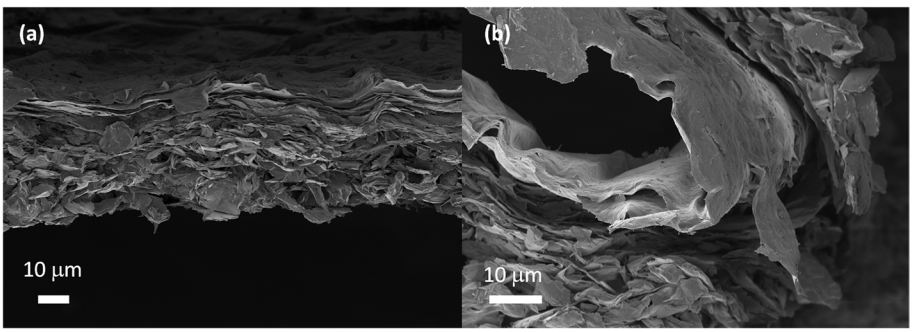

Fig. 4 SEM micrographs of ammonia-modified rectorite film: **a** cross-section view of about 40 µm thick film showing about 10 µm finely layered top and random sheet arrangement through the rest of the profile; **b** continuous top layer of fine parallel clay platelets withstand the banding of the film as oppose to bottom layer seen in process of fracturing

this results in facile crack propagation and ultimately in mechanical failure (Fig. 4).

XRD diffractograms (Fig. 5) show strong first-order basal reflections consistent with well-ordered laminated structures consistent with the SEM observations of the oriented multi-layered films (Fig. 3). Evidence for preferred orientation is also provided by the enhanced intensity and the prominent second and third-order peaks in the diffractograms. Beatrix rectorite is a Na-Ca smectite-mica interstratified structure with d-spacing between 2.18 and 2.22 nm, mean crystallite size in the range 14–21 nm and 6–10 2:1 layers per tactoid (Atanasova et al. 2016). Basal spacing d (001) of 2.22 nm for neat Na-Ca-rectorite corresponds to one water-layer structure with Na^{+}- Ca^{2+} expandable interlayer content in a 3:4 ratio. A reverse trend in the d(001)/d(002) intensity ratio is clearly observed in the diffractograms of the films with the transition from monovalent to

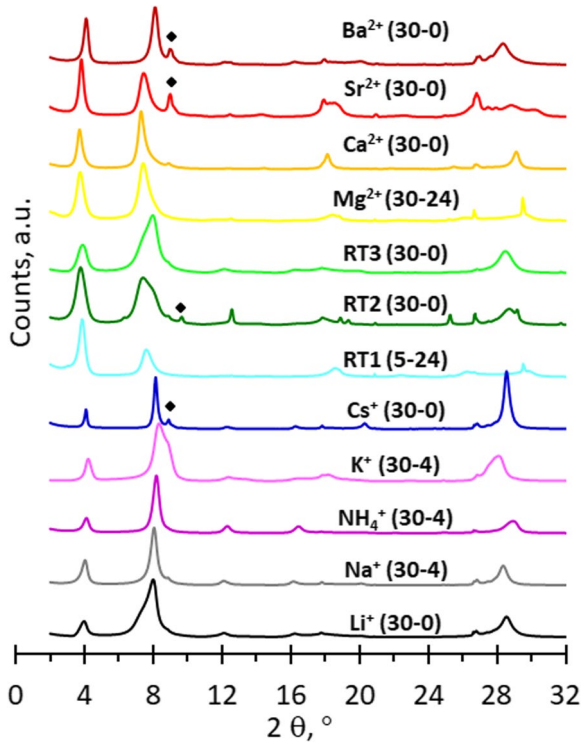

Fig. 5 XRD profiles of films from purified neat Na-Ca-rectorite and exchanged rectorite modifications. The numbers in brackets indicate the dispersion regime. The reflections tagged with the symbol ♦ are due to the presence of a mica impurity

divalent rectorite forms (Fig. 5). This results from differences in scattering efficiency of the monovalent and divalent atoms which is depend on their electron configurations (Moore and Reynolds Jr, 1989). The phenomena have been used to determine the Na/Ca ratio in bi-ionic interlayer structures or other substitutions common in clay minerals using XRD data (Kodama 1966).

Owing to the very high aspect ratios, the average thickness of the platelets comprising the clay films can be estimated from the BET surface area using the equation.

$$t = 2/(\rho \mathrm{A}) \quad (1)$$

where t is the average sheet thickness in m, ρ is the density in kg m^{-3}; and A is the BET surface area in m^2kg^{-1}. Note that Eq. (1) neglects the edge surface area of the flakes. Estimates based on Eq. (1) are presented in Table 4. However, these platelets proved to be imperfect when the crystallite size was considered. One 2:1 layer of rectorite is about 2.20 nm thick consisting of 0.96 nm and 1.30 nm mica- and smectite-type layers respectively stacked along the c direction. The primary tactoids in the natural rectorite consist of up to ten 2:1 silicate layers and have a thickness of about 200 nm (Atanasova et al. 2016). Values based on the XRD-estimated crystallite sizes range from 2 to 6 layers for the tactoids present in the films from neat rectorite and its exchanged modifications.

Table 4 Characteristic physical properties of the rectorite sheets comprising the clay films

Cation	d-spacing	Crystallite size	BET surface area	Flake thickness
	nm	nm	m^2g^{-1}	μm
Li	2.23	6.8	0.286	2.91
Na	2.19	10.8	1.65	0.50
NH_4	2.15	13.7	3.85	0.22
K	2.1	6.5	5.43	0.15
Cs	2.16	12.6	4.21	0.20
RT1	2.16	8.1	1.10	0.76
RT2	2.34	6.9	n.d	-
RT3	2.28	5.7	0.148	5.62
Mg	2.37	9	7.09	0.12
Ca	2.38	8.6	1.39	0.60
Sr	2.32	9.2	4.13	0.20
Ba	2.16	11.2	0.79	1.05

Estimating the ultimate mechanical property values for rectorite films

As mentioned, the presently reported mechanical property measurements do not represent the intrinsic values that might be achieved if the films were defect-free. This prompted the statistical analysis described in the Supplementary information. The outcome of the applied model data fits, together with 95% upper confidence intervals, for these mechanical property values, are listed in Table 5. For comparison, the highest value actually measured in each case is also listed. The values projected by the statistical analysis for the ultimate mechanical properties are not unrealistic. For example, Ballard and Rideal (1983) reported an ultimate tensile strength of 160 MPa and Young's modulus of 14.3 GPa for films made using *n*-butylammonium exchanged vermiculite. This value for the tensile strength is significantly higher than the upper value projected for rectorite-based clay films.

Discussion

The behavior of a rectorite particle in aqueous suspension is defined by its mixed-layer structure and in particular the exchangeable interlayer in the smectite component. The physico-chemical dynamics in the interlayer space of a clay structure in suspension eventually result in swelling and subsequent delamination of the clay

Table 5 Best experimental values for tensile strength and Young's modulus obtained experimentally compared to projected values based on a statistical analysis of the data

Cation type	Experimental[a]	Estimate[b]	95% lower CI	95% upper CI
Tensile strength (MPa)				
Monovalent	44	83	37	129
Divalent	23	48	25	71
Mixed valent	25	49	19	79
Young's modulus (GPa)				
Monovalent	56	97	46	149
Divalent	25	60	29	91
Mixed valent	50	85	32	139

[a] Highest value actually measured

[b] Statistical projection for maximum attainable value

factoids into smaller entities. The interlayer cations diffuse into the double layers around the separated silicate layers in a state of "osmotic swelling" (Lagaly, 2006). The mixed-layer structure of rectorite comprises alternating interlayer spaces with different cation densities, i.e. non-expandable (mica-like) and expandable (smectite-like) layers in a 1:1 ratio with an average CEC of 45 mEq/100 g (Atanasova et al. 2016). The expandable smectite layer is of montmorillonite-beidellite composition and the mica component is of the brittle-micas series paragonite-margarite. Previous NMR and XRD studies of Beatrix rectorite (Atanasova et al. 2016; Jakobsen et al. 1995; Lausen et al. 1999; Vyalikh et al. 2023) reported a high degree of regularity in the layered structure (coefficient of variation for d_{001} of 0.12). A high degree of Al substitution in the mica tetrahedral sheet was established, resulting in the pairing of high-charge top and bottom tetrahedral sheets in a MacEwan crystallite model (MacEwan and Amil 1958; MacEwan 1956, 1957). The mica component layer carries almost a fourfold higher charge density, solely of tetrahedral origin, than the alternating smectite layer. In the latter, the charge is of a dual nature, i.e., partially octahedral from isomorphous substitutions in montmorillonite and partially tetrahedral substitutions in beidellite. Tetrahedral charge is more localized (on three surface oxygens) than octahedral charge resulting in stronger H-bonding of adsorbed H_2O as in micas and vermiculites (Schoonheydt and Johnston 2006). Hence, the bonding strength between silicate layers in the stacking direction of rectorite tactoids is stronger at the mica component layers, resulting in stiffer rectorite lamellae as opposed to smectite-only lamellae. Reportedly this has significant effects on the elastic constant of micas and mica-containing products and ultimately on their mechanical properties (Kunz et al. 2009; Moller et al. 2010). In suspensions, swelling is limited to the smectite interlayers of rectorite. It is also known that monovalent ions facilitate more extensive swelling of the interlayer than divalent ions (Norrish 1954) and that micas do not swell at all (Grim 1968). Consequently, during delamination, the mixed-layer rectorite tactoids will separate only at the low-charged interlayer space, i.e., that of smectite. Theoretically, this process could produce a suspension of "fundamental particles" consisting of a single or just a few mica layers (Nadeau et al. 1985; Srodon et al. 2000) with separation distances in the range of 1 nm, short enough for van der Waals' attraction forces to preserve elementary particle integrity. Furthermore, upon drying and re-assembling the high tetrahedral charge of the outer rectorite layers would promote strong forces bonding the phyllosilicate layers back together. The X-ray diffraction profiles of the dried films (Fig. 5) showed peak positions and ordering identical to the rectorite source material. This indicates that the delaminated layers were re-assembled in an orderly and regular manner and not as random physical mixtures. These results also suggest that dual ordering was attained during the film formation process: at the structure level ordering 2:1 rectorite layers after delamination and the two-dimensional organization of the clay sheets at the film microstructure level.

The role of heterogeneous layer charge

The physicochemical properties of rectorite are defined by the regular alternation of low-charge (smectite) and high-charge (mica) layers and interlayer spaces. The expandable smectite layer controls the thickness and the mica layer and serves to maintain the structural integrity of the rectorite platelet. Within a tactoid unit, the former layer acts as a shear-labile while the latter acts as a shear-stiff reinforcement of the rectorite nanoplatelets (Moller et al. 2010). This functional distribution at a structural level is analogous to other natural mineralized structures such as bone and nacre where ordered arrangements of "soft" and "stiff" phases act synergistically to promote

superior mechanical performance tantamount to advanced engineering materials. The hierarchical arrangement of such layered nanostructures has dramatic effects on the stress and strain propagation in such materials and their derivatives (Dimas and Buehler 2012). The Coulomb attractions between silicate layers and interlayers along the stacking direction are stronger for micas compared to smectites (Kunz et al. 2009) with a strong impact on the mechanical properties of materials containing mica. Hence, when rectorite platelets self-assemble from aqueous suspension the bonding strength along the lamellar stacking and respectively layer stacking in the film organization is stronger than would be expected in smectite suspensions and films.

Finally, it should be mentioned that the effect of cation exchange on the structure and water interactions in these self-assembled rectorite films was previously studied by means of solid-state NMR spectroscopy and electrical impedance spectroscopy (Vyalikh et al. 2023).

Conclusions

The capacity of rectorite to form strong, flexible self-standing clay films in the absence of binders was investigated and the limits for their ultimate material properties were evaluated by a statistical analysis. Clay-only films were prepared by casting aqueous dispersions of exfoliated neat and ion-exchanged rectorite clay through self-assembly during slow evaporation. The clay films consisted of continuous layers of well-aligned clay platelets parallel to the casting surface. Layers appear to be overlapped in a face-to-face fashion in the lateral direction and joined vertically in an irregular manner by face-to-face and edge-to-face bridging to form coherent multi-layered nanostructured films with a platelet-void microstructure. All films showed measurable mechanical properties with some comparing favorably with values exhibited by plastic films used for packaging. Rectorite clay films with monovalent interlayer content exhibited higher strength and stiffness compared to films with divalent modifications and neat Na-Ca-rectorite films. Statistical projections for the maximum attainable values for the mechanical properties indicate that defect-free films could offer significantly better performance.

The presented results highlight the lamellar crystal morphology along with the hybrid layer charge of the mixed-layer structure as the most relevant and unique characteristics of rectorite with regard to its potential to produce strong cohesive films. The large surface area of the clay particles is critical for efficient particle interactions during self-assembly. The increase in the particle aspect ratio was achieved through exfoliation and delamination of the clay tactoids in aqueous suspensions. This is largely dependent on the physico-chemical dynamics in the interlayer space and the nature of the exchangeable interlayer cation in the smectite component of the rectorite structure. XRD of the films confirmed that the delaminated layers reassembled in a regular and orderly manner and not as random physical mixtures, i.e., maintaining the original configuration of pairing high tetrahedral charge of the outer rectorite layers originating from the mica component of the mixed-layer structure. During self-assembly, the thinner tactoids could compact better into textured layered structures due to stronger forces bonding the phyllosilicate layers back together. Hypothetically, the alternating hybrid layer functionality and charge density distribution at the structural level of rectorite domains could synergistically translate at the level of rectorite clay layers reassembling into nanostructured hierarchical films imparting property reinforcement to the nanoplatelets and ultimately render films with strong mechanical performance.

Supplementary Information

The online version contains supplementary material available at https://doi.org/10.1186/s40712-024-00161-z.

Additional file 1: Rectorite clay films

Additional file 2: Self-assembled rectorite films with remarkable mechanical performance: preparation, structural characterization and properties

Acknowledgements

Financial support for this research from the Algeria/South Africa Collaboration Programme of the National Research Foundation (NRF) is gratefully acknowledged. Oliver Woodrow is acknowledged for assisting with the purification and cation exchange process. The authors are indebted to the Council for Geoscience and the University of Pretoria, South Africa for technical support with analytical instrumentation for this research.

Authors' contributions

An optional statement of each author's input into the manuscript, such as conception, experimental design, carrying out measurements, and manuscript composition. CASRAI offers a taxonomy for identifying and describing contributor roles (CRediT). Maria Atanasova: conceptualization; data curation; formal analysis; investigation; methodology; software; supervision; validation; visualization; roles/writing—original draft. Walter Focke: formal analysis; funding acquisition; investigation; project administration; resources; supervision; validation; writing—review and editing. Theo Loots: formal analysis; methodology; software; validation; writing—review and editing. All authors read and approved the final manuscript.

Funding

This research was funded, in part, through the Algeria/South Africa Collaboration Programme of the National Research Foundation (NRF) of South Africa.

Availability of data and materials

Experimental data, in the form of Excel spreadsheets, are available at: https://drive.google.com/drive/folders/1-h4hBBy7tTQuN1fLTMjWvIXuk4XnT-AN?usp=sharing

Declarations

Ethics approval and consent to participate

Ethical approval was not required for this study.

Competing interests

The authors declare that they have no conflicts of interest.

Received: 15 April 2024 Accepted: 2 August 2024
Published online: 13 August 2024

References

Abulyazied DE, Ene A (2021) An investigative study on the progress of nanoclay-reinforced polymers: Preparation, properties, and applications: A review. Polymers 13(24):4401. https://doi.org/10.3390/polym13244401

Anon (1939 Monday, July 24, 1939) Science: Alsifilm Onward. Time Magazine. Retrieved from http://content.time.com/time/magazine/article/0,9171,771687,00.html

ASTM International (2012) ASTM Standard E104, 2002 (2012a) Standard practice for maintaining constant relative humidity by means of aqueous solutions.

ASTM International (2013a) ASTM Standard D618 2013a practice for conditioning plastics for testing.

ASTM International (2013b) ASTM Standard D1708 2013a Standard test method for tensile properties of plastics by use of microtensile specimens ASTM International 2013.

Atanasova MT, Vyalikh A, Scheler U, Focke WW (2016) Characterization of rectorite from the Beatrix Gold Mine in South Africa. Appl Clay Sci 126:7–16. https://doi.org/10.1016/j.clay.2016.02.028

Ballard DGH, Rideal GR (1983) Flexible inorganic films and coatings. J Mater Sci 18(2):545–561. https://doi.org/10.1007/BF00560644

Bennadji-Gridi F, Smith A, Bonnet J (2006) Montmorillonite based artificial nacre prepared via a drying process. Mater Sci Eng B 130:132–136. https://doi.org/10.1016/j.mseb.2006.02.063

Cerbelaud M, Muñoz M, Rossignol F, Videcoq A (2020) Self-Organization of large alumina platelets and silica nanoparticles by heteroaggregation and sedimentation: Toward an alternative shaping of nacre-like ceramic composites. Langmuir 36(13):3315–3322. https://doi.org/10.1021/acs.langmuir.0c00170

Cheary RW, Coelho A (1992) A fundamental parameters approach to X-ray line-profile fitting. J Appl Crystallogr 25(2):109–121. https://doi.org/10.1107/S0021889891010804

Cheng H, Zhou Y, Feng Y, Geng W, Liu Q, Guo W, Jiang L (2017) Electrokinetic energy conversion in self-assembled 2D nanofluidic channels with janus nanobuilding blocks. Adv Mater 29(23):1700177. https://doi.org/10.1002/adma.201700177

Chorom M, Rengasamy P (1995) Dispersion and zeta potential of pure clays as related to net particle charge under varying pH, electrolyte concentration and cation type. European J Soil Sci 46(4):657–665. https://doi.org/10.1111/j.1365-2389.1995.tb01362.x

Dimas LS, Buehler MJ (2012) Influence of geometry on mechanical properties of bio-inspired silica-based hierarchical materials. Bioinspir Biomim 7(3):036024. https://doi.org/10.1088/1748-3182/7/3/036024

Ebina T (2018) Development of Clay-Based Films. Chem Rec 18(7):1020–1032. https://doi.org/10.1002/tcr.201700085

Eguchi M, Konarova ML, Torad N, Chang TA, Kang DY, Shapter J, Yamauchi Y (2022) Highly adhesive and disposable inorganic barrier films: Made from 2D silicate nanosheets and water. J Materials Chem A 10(4):1956–1964. https://doi.org/10.1039/d1ta08837h

Fernandes FM, Baradari H, Sanchez C (2014) Integrative strategies to hybrid lamellar compounds: an integration challenge. Appl Clay Sci 100:2–21. https://doi.org/10.1016/j.clay.2014.05.013

George J, Ishida H (2018) A review on the very high nanofiller-content nanocomposites: Their preparation methods and properties with high aspect ratio fillers. Prog Polym Sci 86:1–39. https://doi.org/10.1016/j.progpolymsci.2018.07.006

Gogoi RK, Raidongia K (2018) Intercalating cation specific self-repairing of vermiculite nanofluidic membrane. J Mater Chem A 6(44):21990–21998. https://doi.org/10.1039/C8TA01885E

Grim RE (1968) Clay Mineralogy (Second ed): McGraw-Hill New York

Hauser EA, Le Beau DS (1938) Studies on gelation and film formation of colloidal clays. I J Phys Chem 42:961–966

Hauser EA, Le Beau DS (1939) Studies on gelation and film formation II Studies in Clay Films. J Phys Chem 43:1037–1048

Jakobsen HJ, Nielsen NC, Lindgreen H (1995) Sequences of charged sheets in rectorite. Am Mineral 80(3–4):247–252. https://doi.org/10.2138/am-1995-3-406

Johnston CT, Santagata M, Sasar M (2022) Chapter 5 Physical and chemical properties of layered clay mineral particle surfaces. In Wypych F, de Freitas RA (Eds.) Developments in Clay Science (Vol. 10 pp. 125–167): Elsevier.

Kaya A, Yukselen Y (2005) Zeta potential of clay minerals and quartz contaminated by heavy metals. Can Geotech J 42(5):1280–1289. https://doi.org/10.1139/t05-048

Kodama H (1966) The nature of the component layers of rectorite. Am Mineral 51(7):1035–1055

Kunz DA, Max E, Weinkamer R, Lunkenbein T, Breu J, Fery A (2009) Deformation measurements on thin clay tactoids. Small 5(16):1816–1820

Lagaly G (2006) Colloid Clay Science. In: Bergaya F, Theng BKG, Lagaly G (Eds.) Handbook of Clay Science (Vol. 1 pp. 141–141).

Lausen SK, Lindgreen H, Jakobsen HJ, Nielsen NC (1999) Solid-state 29Si MAS NMR studies of illite and illite-smectite from shale. Am Mineral 84:1433–1438. https://doi.org/10.2138/am-1999-0922

Liu M-L, Huang M, Tian L-Y, Zhao L-H, Ding B, Kong D-B, Shao J-J (2018) Two-Dimensional Nanochannel Arrays Based on Flexible Montmorillonite Membranes. ACS Appl Mater Inters 10(51):44915–44923. https://doi.org/10.1021/acsami.8b17719

Liu T, Chen B, Evans JR (2008) Ordered assemblies of clay nano-platelets. Bioinspir Biomim 3(1):016005. https://doi.org/10.1088/1748-3182/3/1/016005

Long CT, Chen L, Iverson ET, Castaneda H, Grunlan JC (2022) Cross-linking and silanization of clay-based multilayer films for improved corrosion protection of steel. J Mater Sci 57:2988–2998

Lopes AC, Martins P, Lanceros-Mendez S (2014) Aluminosilicate and aluminosilicate based polymer composites: Present status, applications and future trends. Prog Surf Sci 89(3–4):239–277. https://doi.org/10.1016/j.progsurf.2014.08.002

MacEwan DMC (1956) A study of an interstratified illite-montmorillonite clay from Wocestershire England. Clay J 4:166–172. https://doi.org/10.1346/CCMN.1955.0040122

MacEwan DMC (1957) Fourier transform methods for studying X-ray scattering from lamellar systems. Part II-Interstratifications. Kolloid-Zeitschrift Band 156 . Heft 1 156(1):61–67.

MacEwan DM, Amil AR (1958) Fourier transform methods for studying x-ray scattering from lamellar systems-PartIII-Some effects for clay mineral studies. Kolloid Z 162(9–2):93–100

Minker-Villemin C, Bowen P, Lemaître J, Ring TA (1998) Preparation and properties of potassium-vermiculite films. J Mater Res 13(1):228–236. https://doi.org/10.1557/JMR.1998.0031

Moller MW, Handge UA, Kunz DA, Lunkenbein T, Altsta V, Breu J (2010) Tailoring shear-stiff mika-like nanoplatelets. ACS Nano 4:717–724. https://doi.org/10.1021/nn9011829

Moore DM, Reynolds Jr RC (1989) X-ray diffraction and the identification and analysis of clay minerals: Oxford University Press (OUP).

Nadeau PH, Wilson MJ, McHardy WJ, Tait JM (1985) Interstratified clays as fundamental particles-A reply. Clay Clay Miner 33(6):560. https://doi.org/10.1126/science.225.4665.92

Nam H-J, Ebina T, Ishii RYO, Nanzyo H, Mizukami F (2007) Self-standing film formability of various clays. Clay Sci 13(4–5):159–165. https://doi.org/10.11362/jcssjclayscience1960.13.159

Nam H-J, Ebina T, Mizukami F (2009a) Formability and properties of self-standing clay film by montmorillonite with different interlayer cations. Colloids Surfaces A 346:158–163. https://doi.org/10.1016/j.colsurfa.2009.06.009

Nam H-J, Ishii R, Ebina T, Mizukami F (2009b) Flexible transparent self-standing binderless clay film prepared by hydrothermally-treated synthetic clay. Mater Lett 63(1):54–57. https://doi.org/10.1016/j.matlet.2008.08.057

Norrish K (1954) The swelling of montmorillonite. J Chem Soc Faraday T 18:120–134

Pan X-F, Gao H-L, Lu Y, Wu C-Y, Wu Y-D, Wang X-Y, Yu S-H (2018) Transforming ground mica into high-performance biomimetic polymeric mica film. Nature Commun 9(1):2974. https://doi.org/10.1038/s41467-018-05355-6
Pujala RK, Kumar MP, Dhara S (2018) Hierarchical Self-Assembly of Colloidal Nanoplatelets Driven by Evaporation. Journal of Physics D: Appl Phys 51:304003. https://doi.org/10.1088/1361-6463/aacacd
Saha K, Deka J, Gogoi RK, Datta KKR, Raidongia K (2022) Applications of lamellar membranes reconstructed from clay mineral-based nanosheets: A Review. ACS Appl Nano Mater 5(11):15972–15999. https://doi.org/10.1021/acsanm.1c03207
Schoonheydt R (2014) Functional hybrid clay mineral films. Appl Clay Sci 96:9–21. https://doi.org/10.1016/j.clay.2014.04.010
Schoonheydt RA, Johnston CT (2006) Surface and interface chemistry of clay minerals. In: Bergaya F, Theng BKG, Gerhard Lagaly G, Developments in Clay Science, Elsevier (2006) 1:87–113.https://doi.org/10.1016/S1572-4352(05)01003-2
Sellinger A, Weiss MP, Nguyen A, Lu Y, Assink RA, Gong W, Brinker CJ (1998) Continuous self-assembly of organic-inorganic nanocomposite coatings that mimic nacre. Nature 394:256–260. https://doi.org/10.1038/28354
Shao J-J, Raidongia K, Koltonow AR, Huang J (2015) Self-assembled two-dimensional nanofluidic proton channels with high thermal stability. Nat Commun 6(1):7602. https://doi.org/10.1038/ncomms8602
Srodon J, Eberl DD, Drits VA (2000) Evolution of fundamental particle size during illitization. Clay Clay Miner 48:446–458. https://doi.org/10.1346/CCMN.2000.0480405
Stokes AR, Wilson AJC (1942) A method of calculating the integral breadths of Debye-Scherrer lines. Math Proc Cambridge 38(03):313–322. https://doi.org/10.1017/S0305004100021988
Tjong SC (2006) Structural and mechanical properties of polymer nanocomposites. Mater Sci Eng R: Reports 53(3–4):73–197. https://doi.org/10.1016/j.mser.2006.06.001
Vyalikh A, Atanasova MT, Focke WW, Makarova AA, Krajnc A, Mali G (2023) Investigation of the structural and electrical conductivity properties in pure and cation exchanged rectorite. Appl Clay Sci 245:107116. https://doi.org/10.1016/j.clay.2023.107116
Walker GF, Garrett WG (1967) Chemical Exfoliation of Vermiculite and the Production of Colloidal Dispersions. Science 156(3773):385–387. https://doi.org/10.1126/science.156.3773.385
Walley P, Zhang Y, Evans JR (2012) Self-assembly of montmorillonite platelets during drying. Bioinspir Biomim 7(4):046004. https://doi.org/10.1088/1748-3182/7/4/046004
Wang YC, Lin JJ (2014) Clay films with variable metal ions and self-assembled silicate layer-void nanostructures. RSC Adv 4(12):6356–6362. https://doi.org/10.1039/c3ra46628k
Wang YC, Huang TK, Tung SH, Wu TM, Lin JJ (2013) Self-assembled clay films with a platelet-void multilayered nanostructure and flame-blocking properties. Sci Rep 3:2621
Xiao T, Liu Q, Zhang Q, Liu Z, Zhai J (2017) Temperature and voltage dual-responsive ion transport in bilayer-intercalated layered membranes with 2D nanofluidic channels. J Phys Chem C 121(34):18954–18961. https://doi.org/10.1021/acs.jpcc.7b06245
Xie W, Wang J, Fu L, Tan Q, Tan X, Yang H (2020) Evolution of the crystallographic structure and physicochemical aspects of rectorite upon calcination. Appl Clay Sci 185:105374. https://doi.org/10.1016/j.clay.2019.105374
Zhang Y, Evans JRG (2012) Approaches to the manufacture of layered nanocomposites. Appl Surf Sci 258:2098–2102. https://doi.org/10.1016/j.apsusc.2011.03.151
Zhou CH, Shen Z-F, Liu LH, Liu SM (2011) Preparation and functionality of clay-containing films. J Mater Chem 21(39):15132–15153. https://doi.org/10.1039/C1JM11479D
Zhou Y, Ding H, Smith AT, Jia X, Chen S, Liu L, Sun L (2019) Nanofluidic energy conversion and molecular separation through highly stable clay-based membranes. J Mater Chem A 7(23):14089–14096. https://doi.org/10.1039/C9TA00801B
Zimmerman JB, Anastas PT, Erythropel HC, Leitner W (2020) Designing for a green chemistry future. Science 367(6476):397–400. https://doi.org/10.1126/science.aay3060

Publisher's Note